NANO: Brief Reports and Reviews
Vol. 6, No. 5 (2011) 469–479

DOI: 10.1142/S1793292011002846

A FACILE SYNTHESIS OF SHAPE- AND SIZE-CONTROLLED α-Fe_2O_3 NANOPARTICLES THROUGH HYDROTHERMAL METHOD

GUANG-HUI WANG, WEN-CUI LI, KUN-MING JIA and AN-HUI LU*
State Key Laboratory of Fine Chemicals
School of Chemical Engineering
Dalian University of Technology
Dalian 116024, P. R. China
**anhuilu@dlut.edu.cn*

MATHIAS FEYEN, BERND SPLIETHOFF and FERDI SCHÜTH
Max-Planck-Institut für Kohlenforschung
D-45470 Mülheim an der Ruhr, Germany

Received 31 May 2011
Accepted 19 July 2011

α-Fe_2O_3 nanoparticles have wide-ranging applications such as in catalysis, sensoring, painting, etc. This is the reason to study their controlled synthesis. Here we have investigated the synthesis of uniform α-Fe_2O_3 nanoparticles using amino acids as morphology control agents. The products were characterized by transmission electron microscopy (TEM), X-ray diffraction (XRD), thermogravimetry (TG) and differential thermal analysis (DTA). It was found that the type and the amount of amino acids as well as the reaction temperatures have significant influence on the shape and size of the obtained α-Fe_2O_3 nanoparticles. The use of acidic amino acids (always contain C=O in the side chain) typically leads to the formation of α-Fe_2O_3 nanoparticles with spindle shape. However, rhombohedrally shaped α-Fe_2O_3 nanoparticles were formed in presence of basic amino acids (always contain $-NH_2$ in the side chain). Increasing the amount of amino acid generally results in α-Fe_2O_3 nanoparticles with decreasing particle sizes.

Keywords: Hematite; nanocrystals; amino acids; hydrothermal method.

1. Introduction

Hematite (α-Fe_2O_3) is the most stable iron oxide under ambient conditions. Owing to its low cost and high resistance to corrosion, it has widespread applications, for instance, as catalyst,[1] gas sensor[2] and electrode material.[3] In the past decades, different α-Fe_2O_3 nanostructures, such as spheres,[4,5] rods,[6] cubes,[7] tubes,[8] belts[9] or rings[10] have been synthesized. It is well-known that the shape and size of α-Fe_2O_3 nanoparticles have a great impact on their chemical and physical properties such as, on magnetic[11,12] and catalytic properties.[13,14] The size- and shape-dependent properties of hematite nanoparticles have stimulated much effort towards the controlled synthesis of α-Fe_2O_3 nanoparticles. So far, various methods including the sol–gel process,[6] thermal oxidation of iron metal,[9] the hydrothermal approach[4,15] and thermal decomposition[2,16] have been used to prepare α-Fe_2O_3 nanoparticles. Among these methods, hydrothermal synthesis, which can initiate nucleation of high numbers of nuclei to form crystalline nanoparticles

at low temperatures, has become an important and promising approach to prepare controlled inorganic nanocrystals.[17,18] Recently studies on the controlled synthesis of α-Fe_2O_3 nanoparticles by hydrothermal methods, assisted by various capping agents have been reported. Pu and co-workers have used the cationic surfactant CTAB as capping agent to mediate the hydrolysis of $FeCl_3$. By changing the molar ratio between CTAB and $FeCl_3$, they have obtained α-Fe_2O_3 with different shapes including nanosized rhombohedra, nanorods and nanocubes.[19] Gao's group developed a simple hydrothermal synthesis of single-crystalline α-Fe_2O_3 submicron-cubes with edge lengths in the range of 500–800 nm, also using CTAB as the capping agent.[20] In the presence of $NH_4H_2PO_4$, α-Fe_2O_3 nanotubes (outer diameters of 90–110 nm, inner diameters of 40–80 nm and lengths of 250–400 nm) can be obtained by the hydrothermal treatment of $FeCl_3$ solution.[8] Cao's group has reported a hydrothermal synthesis of rice and cube-shaped α-Fe_2O_3 via a reaction between $Fe(NO_3)_3 \cdot 9H_2O$ and $NH_3 \cdot H_2O$ in ethylene glycol.[21] Hydrothermal synthesis assisted with oleic acid in a mixture of ethanol and water solution resulted in α-Fe_2O_3 nanocubes with sides of 20 nm.[4] Amino acids (L-phenylalanine, L-serine, L-alanine, L-glutamine, L-glutamic acid) were also used as reactants for the synthesis of spherical and ellipsoidal α-Fe_2O_3.[22] However, except for amino acids, HCl was used to control the pH of the solution, while the influence of HCl on the morphology of the hematite nanoparticles cannot be ruled out.[23] Moreover, in this synthesis, the hydrothermal reaction temperature was only limited at 100°C.

Very recently, we have demonstrated that spindle- and rhombohedral-shaped α-Fe_2O_3 nanoparticles with different sizes can be synthesized with the assistance of asparagine and lysine.[13] It was found that in the gold catalyzed CO oxidation, spindle shape iron oxide supports result in higher catalytic activity than rhombohedral-shaped ones of the same size. This finding led to a systematic exploration of the influence of amino acids on the synthesis of α-Fe_2O_3 nanoparticles. In the present study, various amino acids were used as additives in order to study the influence of amino acids on the morphology of hematite nanoparticles. In addition, the influence of the hydrothermal temperatures on the size and morphology of the α-Fe_2O_3 nanoparticles was investigated.

2. Experimental Section

2.1. *Materials*

Ferric chloride hexahydrate ($FeCl_3 \cdot 6H_2O$) was purchased from Alfa-Aesar. The L-glutamic acid, L-aspartic acid, L-lysine and D-asparagine were obtained from Fluka. All chemicals were used as received without further purification. The water used in this work was distilled.

2.2. *Synthesis of α-Fe_2O_3 nanoparticles*

In a typical procedure, 0.002 mol of $FeCl_3 \cdot 6H_2O$ and the respective amount of glutamic acid were firstly dissolved in 100 mL distilled water under vigorous stirring at room temperature for 2 h to form a clear solution with gradual change in color from yellow to dark red depending on how much glutamic acid was used. The molar ratios of [Fe^{3+}]/[glutamic acid] were varied from 1:0.05 to 1:0.1, 1:0.25, 1:0.5 and to 1:1. The pH values of the solution were in the range of 1.89–1.93 (measured by CyberScan pH300/310). Subsequently, the mixture was transferred to a Teflon-lined stainless steel autoclave of 150 mL capacity, sealed and maintained at a given temperature in the range 100–200°C for 24 h. Afterwards, the autoclave was allowed to cool down to room temperature. The resulting reddish products were collected by centrifugation, washed three times with distilled water and once with absolute ethanol and finally dried in an oven at 50°C for 4 h. In the cases of using aspartic acid, lysine and asparagine as the reactants, the synthetic conditions are essentially the same as above except that glutamic acid was replaced by other amino acids. The pH values of all the solution using different amino acids are about 2. Further detailed information will be given in the corresponding context.

2.3. *Characterization*

The powder X-ray diffraction (XRD) was performed on a Rigaku D/Max-2400 X-ray diffractometer (Cu Kα radiation, $\lambda = 1.5432$ Å). Transmission electron microscopy (TEM) analyses were carried out with Tecnai $G^2$20S-Twin equipment operating at 200 kV. Part of the TEM images were measured with a Hitachi HF 2000 transmission electron microscope operated at 200 kV. The samples for TEM analysis were prepared by dipping the carbon-coated copper grids into the ethanol solutions of hematite nanoparticles and drying at room temperature.

Thermogravimetic analysis (TGA) was performed on a NETZSCH STA 449C thermobalance. The measurement was carried out under air with a heating rate of 10°C/min.

3. Results and Discussion

Amino acids are molecules containing both amine and carboxyl functional groups with the general formula H2NCHRCOOH, thus the amino acid simultaneously provides both functionalities. Here we chose four kinds of amino acids of different character including glutamic acid and aspartic acid (acidic), lysine (basic) and asparagine (nearly neutral) which differ from each other in the side chain attached to their alpha carbon. For all the syntheses, the Fe^{3+} content was maintained as 0.02 M. Other synthetic conditions such as the type and the amount of the amino acids and the temperatures of hydrothermal treatment were varied. The detailed conditions for the preparation of samples are listed in Table 1. Using these amino acids as reactants, reddish particles were collected by centrifugation after hydrothermal synthesis at temperature of 100°C or higher.

Essentially, the XRD patterns of all synthesis products showed similar reflections. For simplicity, only four representative XRD patterns of synthesized iron oxide nanoparticles are displayed in Fig. 1. The patterns can unambiguously be assigned to α-Fe_2O_3 (JCPDS Card No. 33-664). The sharp peaks indicate that the α-Fe_2O_3 nanoparticles are highly crystalline without other detectable impurities. Obviously, at aging temperature over 100°C the stable α-Fe_2O_3 phase can be formed, which is in agreement with a report in the literature.[24]

Figure 2 shows the TEM images of α-Fe_2O_3 nanoparticles synthesized with glutamic acid at various [Fe^{3+}]/[glutamic acid] molar ratios of 1:0.05, 1:0.1, 1:0.5 and 1:1, respectively. Glutamic acid contains one carboxyl group at the end of the side chain in addition to the primary carboxyl group and is negatively charged under neutral conditions. The pH values of the aqueous solution consisting of glutamic acid and $FeCl_3 \cdot 6H_2O$ are in the range of 1.89–1.93, which are slightly lower than the pH value (1.95) of the solution only containing $FeCl_3 \cdot 6H_2O$. With increasing amount of glutamic acid used, the shapes of the resultant α-Fe_2O_3 nanoparticles gradually vary from nearly spherical (S1, see Fig. 1(a)) to ellipsoidal (S2, see Fig. 1(b)), to spindle-like (S3, see Fig. 1(c)) nanocrystals and their corresponding aspect ratios (defined as the length of the major axis (c) divided by the width of the minor axis (a)) are 1.0, 1.5 and 1.9, respectively.

Table 1. Experimental conditions for the preparation of samples.

Sample	Amino acid	Molar ratio [Fe^{3+}]/[amino acid]	Temp °C	Size[a] (c) nm	Aspect ratio (c/a)	Morphology
S1	glutamic acid	1:0.05	100	140–155	1.0	sphere
S2	glutamic acid	1:0.1	100	170	1.5	ellipsoid
S3	glutamic acid	1:0.5	100	117	1.9	spindle
S4	glutamic acid	1:1	100	82; 40	1.9; 5.7	spindle; rod
S5	glutamic acid	1:1	200	70–80	1.0	sphere
S6	glutamic acid	1:0.25	200	70–80	1.0	sphere
S7	glutamic acid	1:0.25	150	50–100	—	sphere; spindle
S8	aspartic acid	1:0.05	100	173	1.6	spindle
S9	aspartic acid	1:0.1	100	166	1.8	spindle
S10	aspartic acid	1:0.25	100	157	2.0	spindle
S11	aspartic acid	1:0.5	100	40	5.7	rod
S12	aspartic acid	1:0.25	120	130–200	1.8	spindle
S13	aspartic acid	1:0.25	150	120–180	1.6	spindle
S14	lysine	1:1	120	115–130	1.4	rhombohedra
S15	lysine	1:1	150	110–130	1.3	rhombohedra
S16	lysine	1:1	180	105–130	1.2	rhombohedra
S17	asparagine	1:1	120	—	—	—
S18	asparagine	1:1	150	80—130	—	spindle
S19	asparagine	1:1	180	40—130	—	spindle

[a]To describe the sizes of crystals, the length of the major axis (c) of hematite nanoparticles is used.

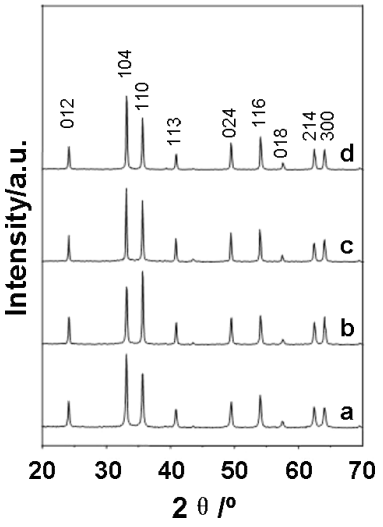

Fig. 1. XRD patterns of the synthesized products: (a) S1, (b) S3, (c) S10 and (d) S13.

When the molar ratio of $[Fe^{3+}]$/[glutamic acid] reaches 1:1, α-Fe_2O_3 nanoparticles were prepared as a mixture of spindles and rods (S4, see Fig. 1(d)).

Besides the variation of shapes, the sizes of the hematite nanoparticles decrease obviously when increasing the amount of glutamic acid (combining the TEM observations and the data in Table 1). Additionally, it is noteworthy that the α-Fe_2O_3 nanoparticles synthesized under various reaction conditions can be easily redispersed in water as stable colloidal suspension. It can be concluded that the glutamic acid plays an important role in defining the shape and the size of the α-Fe_2O_3 nanoparticles during hydrothermal synthesis.

It is well-known that the hydrolysis temperature influences the nuclei formation as well as growth kinetics, thus also affecting the particle size and morphology of the resultant inorganic nanoparticles. It should be noted that with glutamic acid as additive and synthesis temperatures exceeding 230°C, only nondispersed black particles were found on the bottom of the Teflon liner after one day of aging; no reddish nanoparticles were obtained. Thus, 200°C was selected as the maximum treatment temperature for the other experiments. Taking the same reaction conditions as for sample S4, sample S5 was synthesized at an aging temperature of 200°C. The TEM image [Fig. 3(a)] of this sample shows that the nanocrystals mainly consist of

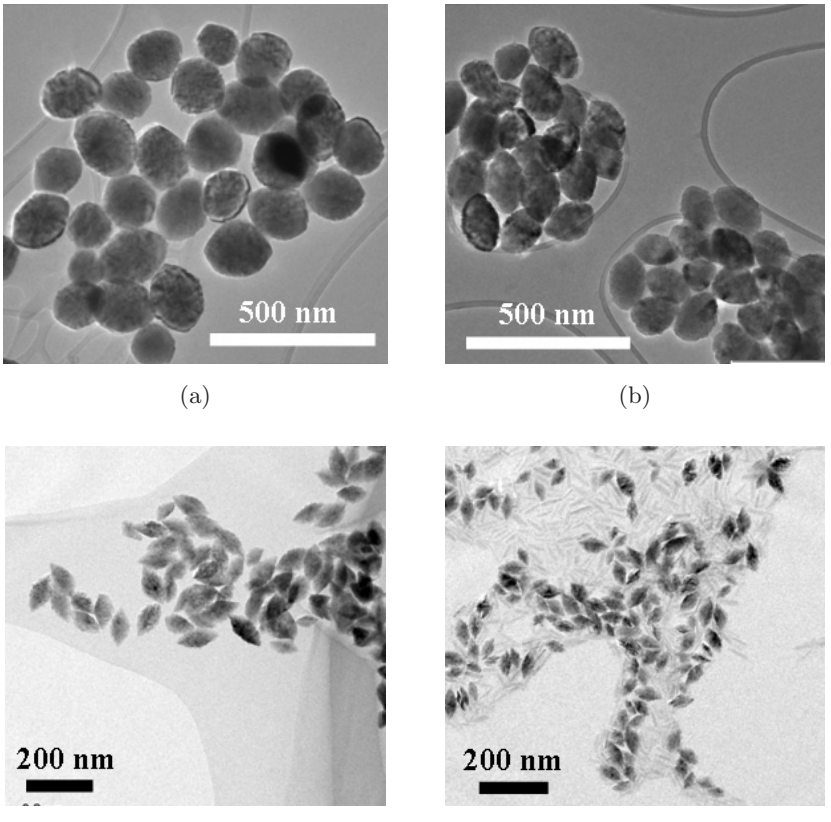

(a) (b)

(c) (d)

Fig. 2. TEM images of α-Fe_2O_3 nanoparticles synthesized using glutamic acid: (a) S1, (b) S2, (c) S3 and (d) S4.

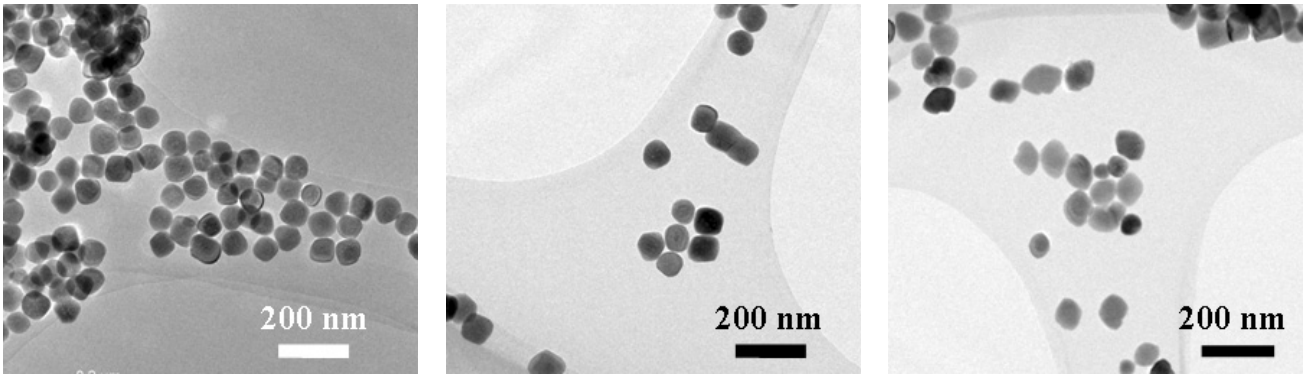

(a) (b) (c)

Fig. 3. TEM images of α-Fe_2O_3 nanoparticles synthesized using glutamic acid: (a) S5, (b) S6 and (c) S7.

nearly spherically shaped particles with relatively uniform size distribution (70–80 nm), no spindle- or rod-shaped particles were found. This indicates that the hydrothermal aging temperature also has a remarkable influence on the shape of the nanoparticles. By decreasing the amount of glutamic to $[Fe^{3+}]$/[glutamic acid] molar ratio of 1:0.25 and maintaining the hydrothermal aging temperature at 200°C, no substantial changes were observed for the obtained α-Fe_2O_3 nanoparticles (S6, see Fig. 3(b)), indicating that the amount of amino acid is less important in directing the shape and size of α-Fe_2O_3 nanoparticles at high aging temperature. Furthermore, by reducing the hydrothermal aging temperature to 150°C and maintaining the $[Fe^{3+}]$/[glutamic acid] molar ratio of 1:0.25, the resulting α-Fe_2O_3 nanoparticles exhibited various shapes like spindles and spheres with a broad size distribution from 50 to 100 nm (S7, see Fig. 3(c). These results indicate that higher aging temperatures lead to relatively equal growth rates of nanocrystals from different faces. It is thus more difficult to control particle shape at high synthesis temperature.

Another acidic amino acid, D-aspartic acid with short carbon chain was also applied as additive to perform the hydrothermal synthesis of α-Fe_2O_3 nanoparticles. As seen in Figs. 4(a)–4(c), the resulting α-Fe_2O_3 nanoparticles of sample S8, S9 and S10 are obtained as spindle-like crystals. Moreover, the aspect ratios of these samples increased from 1.6 and 1.8 to 2 with increase in the amount of aspartic acid, while the sizes of the products decreased from 173 and 166 to 157 nm (see Table 1). When the molar ratio of $[Fe^{3+}]$/[aspartic acid] reaches 1:0.5 (S11, see Fig. 4(d)), the morphology of α-Fe_2O_3 nanoparticles changes to rod shape. This indicates that aspartic acid also influences the morphology of the α-Fe_2O_3 nanoparticles, while the qualitative change of the shape with increasing concentration of additives is identical to the one observed with glutamic acid: higher concentration leads to more elongated and smaller particles. By fixing the molar ratio of $[Fe^{3+}]$/[aspartic acid] at 0.25 and increasing the hydrothermal aging temperature from 100°C to 120°C and 150°C, the resulting α-Fe_2O_3 nanoparticles (S12 and S13, see Figs. 4(e) and 4(f)) still exhibit spindle-shaped morphology, but the aspect ratios of the two samples decrease to 1.8 and 1.6, respectively. One can deduce that, in the case of aspartic acid, higher aging temperatures also lead to relatively equal growth rates of nanocrystals from different faces. Compared with the results of hematite nanoparticles prepared with aspartic acid and glutamic acid, it appears that the two kinds of amino acids have a similar effect in the formation of α-Fe_2O_3 nanoparticles, i.e., the particles exhibit spindle-like shapes at small concentrations of amino acid and the particle sizes decrease with increasing concentration of amino acid. At further increased concentration of amino acid, rod-like nanoparticles are obtained. Although aspartic acid and glutamic acid are both acidic amino acids, the former one leads to the formation of nanoparticles with a much higher aspect ratio than the latter. Thus, by selecting proper synthetic conditions, it is possible to synthesize α-Fe_2O_3 nanoparticles with certain shapes such as nearly spherical, spindle and rod type nanocrystals. More importantly, under those synthetic conditions, the obtained α-Fe_2O_3 nanoparticles are single crystals. A representative selected area electron diffraction patterns (SAED) depicted in Fig. 4(h) proves the single crystalline nature of the products. For this sample, the average

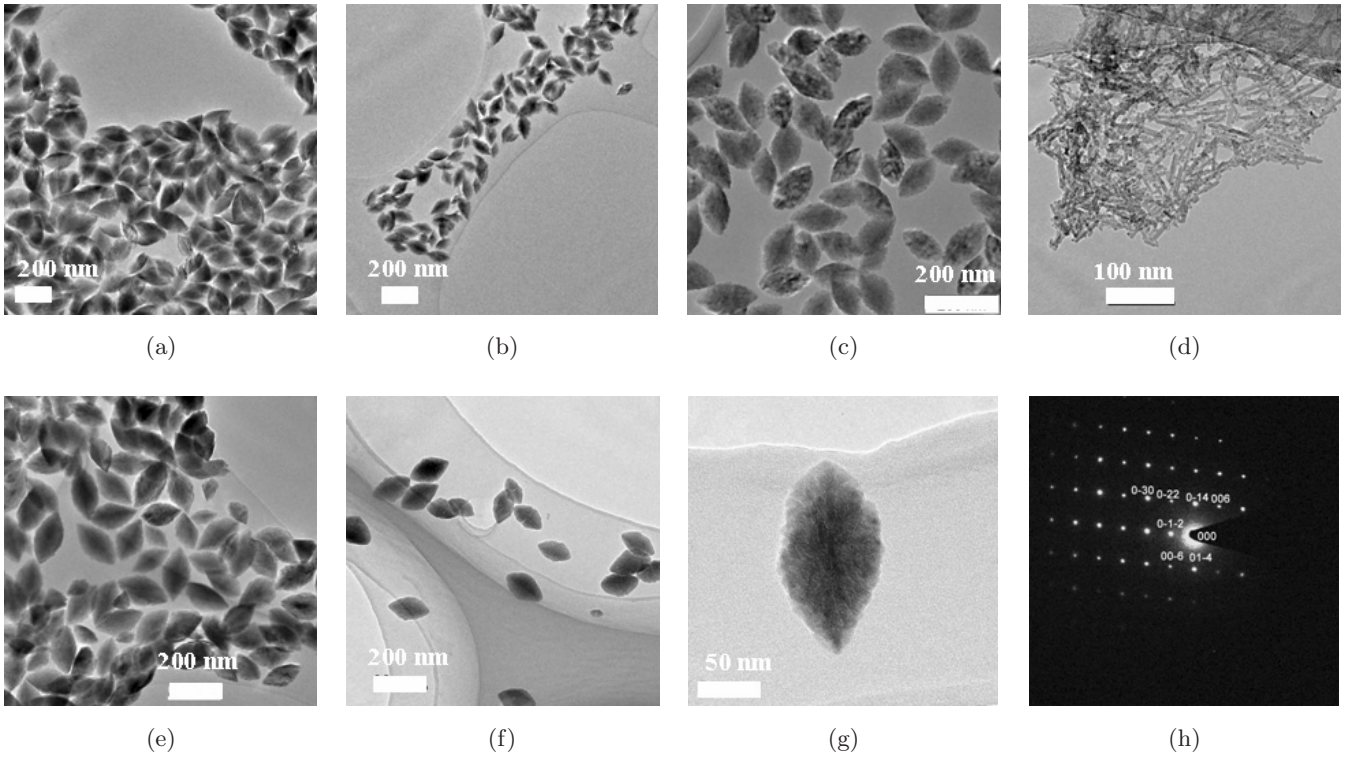

Fig. 4. TEM images of α-Fe_2O_3 nanoparticles prepared using aspartic acid: (a) S8, (b) S9, (c) S10, (d) S11, (e) S12, (f) S13, (g) single particle from sample (c) and (h) the SAED of particle (g).

particle sizes determined from TEM are around 79 nm × 157 nm in width and length. The average particle size calculated from the Scherrer equation based on the XRD pattern is about 75 nm, in reasonable agreement with the size determined by TEM also supporting the single-domain nature of the particles. The elemental composition of the products examined by energy-dispersive X-ray analysis (EDX) confirmed the presence of Fe and O with the expected ratio of 2:3.

Besides using acidic amino acid as the reactants, we have also used the basic amino acid L-lysine as the additive to synthesize iron oxide nanoparticles. The pH values of this solution are in the range of 2.04–2.38. As described in the previous paper,[13] it was found that using lysine as the additive, at an aging temperature of 120°C rhombohedral α-Fe_2O_3 nanoparticles were obtained. With the increase of the amount of lysine used, the particle size decreases. The resultant nanoparticles have different shape as compared to those particles synthesized with acidic amino acids which is obviously due to the effect of lysine. When the reaction temperature is increased from 120°C to 150°C and 180°C at the $[Fe^{3+}]$/[lysine] molar ratio of 1:1, the aspect ratio of the products gradually decreases from 1.4 to 1.3 and 1.2, while the length of the major axis (c) of the particles has no significantly change (S14, S15 and S16, see Figs. 5(a)–5(c)). This indicates that, similar as for the acidic amino acids, higher aging temperatures also lead to relatively equal growth rates of nanocrystals from different faces which results in the decrease of aspect ratios.

Asparagine is a neutral amino acid and has only the amino group and the carboxyl groups which make it an amino acid. The pH values of the aqueous solution consisting of D-asparagine and $FeCl_3 \cdot 6H_2O$ are about 1.91–2.02. In general, using D-asparagine as the additive for synthesis of α-Fe_2O_3 nanoparticles, similar morphologies were observed as with acidic amino acids. With the increase of the amount of asparagine used, the particle size decreases.[13] Small particles are more desirable in catalysis because of their increased surface area. Here, a higher amount of asparagine ($[Fe^{3+}]$/[D-asparagine] molar ratio of 1:1) was used to prepare α-Fe_2O_3 nanoparticles at different aging temperature of 120°C, 150°C and 180°C. At an aging temperature of 120°C, uniformly distributed primary nanoparticles with a size of ∼10 nm and spindle-like nanocrystals were observed (S17, see

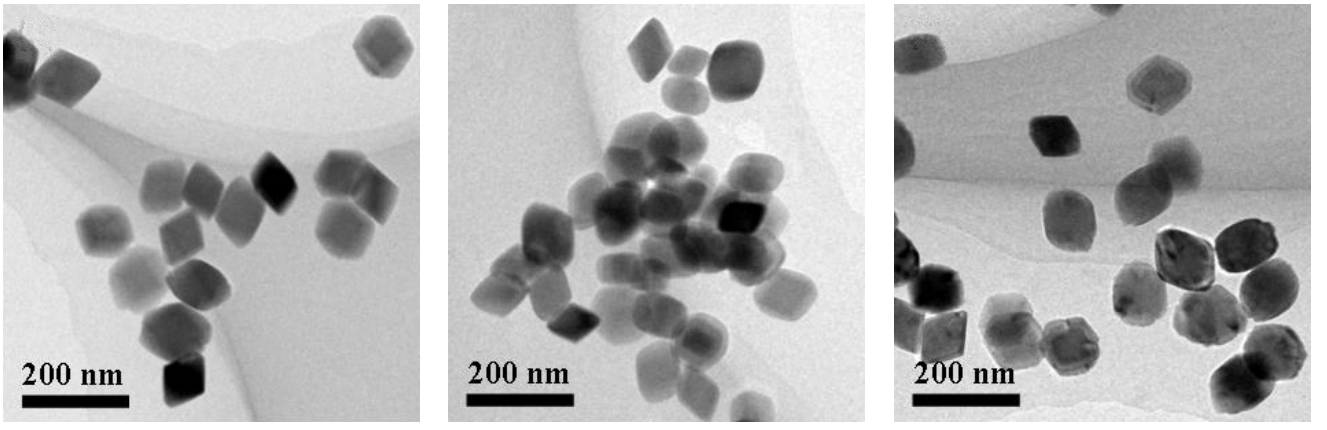

(a) (b) (c)

Fig. 5. TEM images of α-Fe_2O_3 nanoparticles prepared using lysine: (a) S14, (b) S15 and (c) S16.

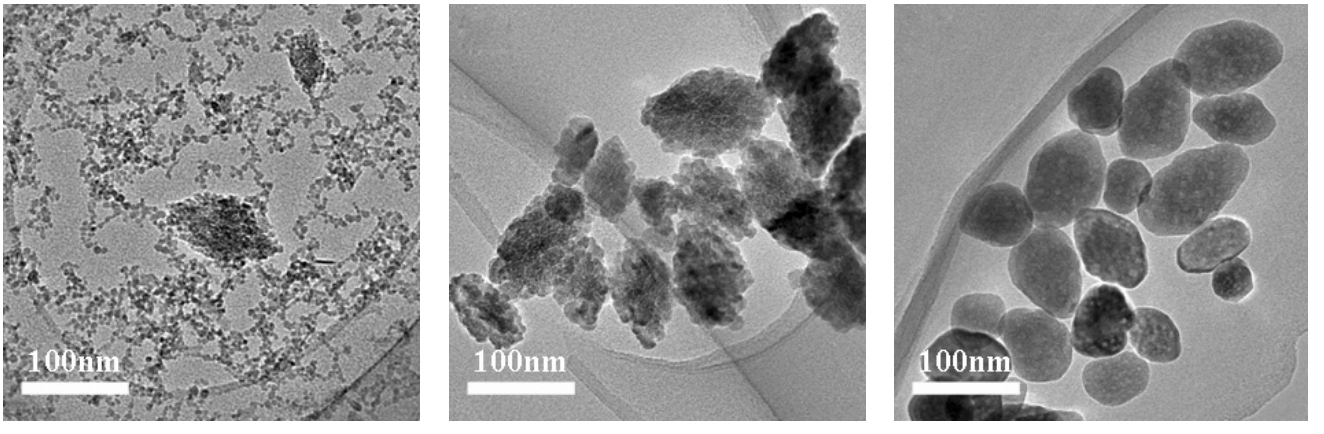

(a) (b) (c)

Fig. 6. TEM images of α-Fe_2O_3 nanoparticles synthesized using asparagine: (a) S17, (b) S18 and (c) S19.

Fig. 6(a)), which may suggest that during the hydrothermal aging period, these 10 nm primary particles self-assembled into the spindle structured α-Fe_2O_3 nanoparticles. At an aging temperature of 150°C, the edge of the spindle coarsened (S18, see Fig. 6(b)). Increasing the temperature to 180°C, the α-Fe_2O_3 nanoparticles essentially kept the spindle shape. However, it seems that the primary nanoparticles at the edge of the spindle tend to fuse together and many pores appear on the surface of the hematite nanoparticles (S19, see Fig. 6(c)). Figure 7 shows the nitrogen sorption isotherm and pore size distribution of the sample of S19. Its BET surface area is around 40 m^2/g, witch is much higher than that reported in literature.[13] The average pore size, as calculated from desorption branch of the nitrogen isotherm by the BJH method, is about

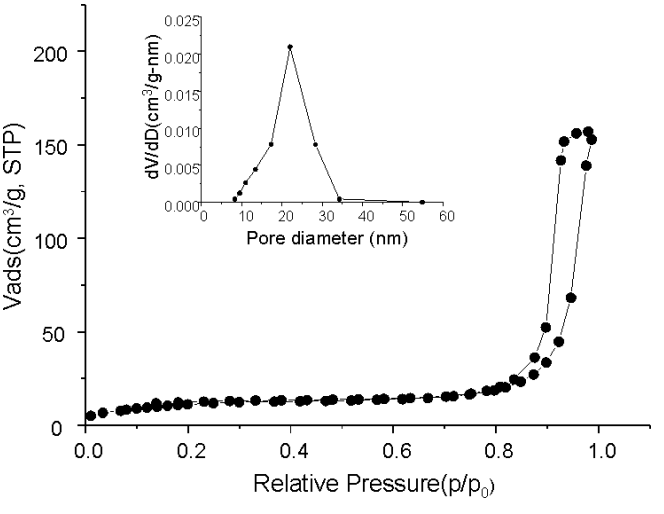

Fig. 7. Nitrogen sorption isotherm with the pore diameter distribution (inset) of S19.

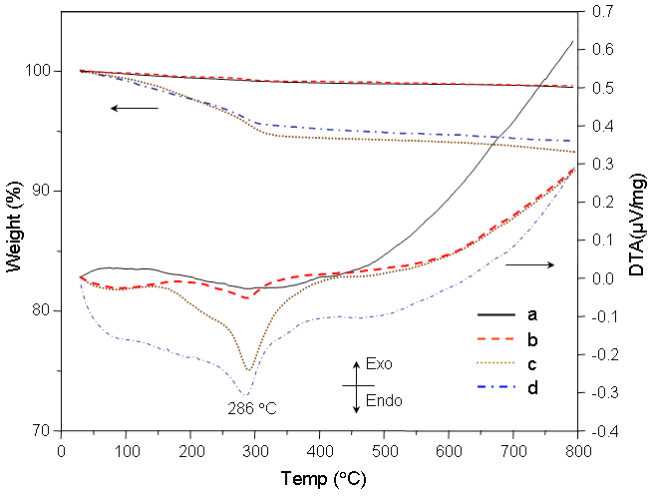

Fig. 8. TG and DTA of α-Fe_2O_3 nanoparticles synthesized without amino acid (a), with amino acids: lysine (b), glutamic acid (c) and asparagine (d).

21 nm which can be attributed to the accumulation pores between particles.

Since a constant amount of Fe^{3+} was used, the change in size and shape of the resulting particles has to be attributed to the influence of the amino acids. In the absence of amino acids, the products are known to have a broad size distribution and irregular shapes[19] (Our data also show this fact, as shown in Fig. 9(a)). Based on the above mentioned facts, the conclusion can clearly be drawn that amino acids are effective in determining the morphology and the size of the α-Fe_2O_3 crystals. At higher aging temperature, the type and the amount of amino acids are less important in directing the shape and size of α-Fe_2O_3 nanoparticles. To examine the differences of the resultant hematite nanoparticles from different amino acids, hematite synthesized using acidic (glutamic acid, 100°C aged), neutral (asparagine, 120°C aged) and basic (lysine, 120°C aged) amino acids as examples were characterized in more detail by TG and TEM. Hematite nanoparticles synthesized without amino acid additives (aged at 100°C, the other synthetic conditions are the same as the one prepared with an amino acid) was used as a reference. Thermogravimetry (TG) and differential thermal analysis (DTA) measurements were carried out in a thermobalance in order to compare the different steps in the thermal evolution of the hematite nanoparticles. As can be seen in Fig. 8, α-Fe_2O_3 crystals synthesized with lysine and without amino acid (aged only

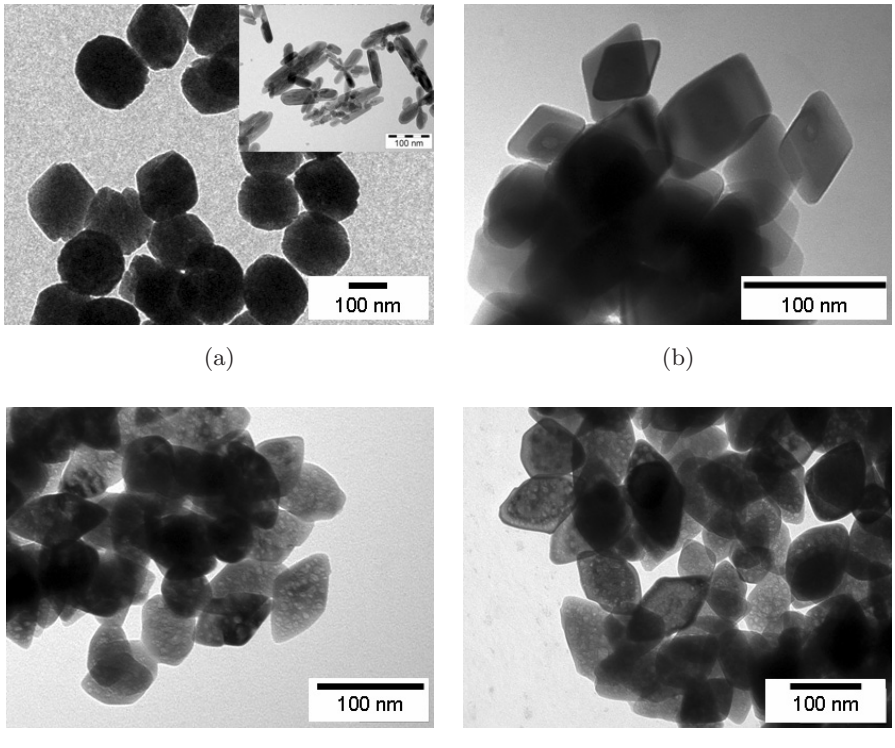

(a) (b)

(c) (d)

Fig. 9. TEM images of α-Fe_2O_3 nanoparticles after calcination at 350°C. The α-Fe_2O_3 nanoparticles were synthesized without amino acid (inset is the TEM image of the iron oxides from the mother solution) (a), with amino acids: lysine (b), glutamic acid (c) and asparagine (d).

in water at 100°C for 24 h) show similar thermal behavior, the two TG curves are almost overlapping and the weight loss is less than 1.0 wt.% in both samples up to temperatures of 350°C. However, α-Fe_2O_3 crystals synthesized using glutamic acid and asparagine show remarkable weight losses (about 4.6 wt.% and 5.4 wt.%, respectively) below 350°C. From 350°C to 800°C, the weight loss is 1.2 wt.% for both samples, indicating an identical thermal evolution of the crystal structure. It is noteworthy that the α-Fe_2O_3 synthesized with amino acids all show endothermic peaks at around 285°C in the DTA trace. This signal may relate to the condensation of free hydroxyl groups or recrystallization of the iron oxide nanoparticles. Since the major weight loss occurs before 350°C, we calcined the as-synthesized α-Fe_2O_3 crystals at 350°C for 4 h in air. As seen in Fig. 9, the TEM images reveal that both the spindle and rhombohedrally shaped nanocrystals retained their original morphologies after calcination. Interestingly, the spindle-shaped crystals (synthesized with glutamic acid or asparagine) developed visible holes in the calcined particles which is attributed to the combustion of the surface adsorbed small amount organic molecules and the condensation of hydroxyl groups.

From the details mentioned above, one type of formation mechanism can be proposed for the growth of hematite nanoparticles in the presence of amino acids, namely, "nucleation–aggregation–recrystallization" which is consistent with the cases using CTAB[19,20] and PO_4^{3-} ions[25] as capping agents (Fig. 10). In the formation process, amino acids as additives can preferentially adsorb on specific faces to stabilize nonequilibrium morphologies by changing the relative growth rates of different crystal faces. At low temperature, the amino acid and Fe^{3+} cations can form complexes through the chelating groups like –NH_2 and –COOH. During the hydrothermal synthesis, hydrated Fe^{3+} cations undergo hydrolysis to form FeOOH and then further condense to α-Fe_2O_3 nuclei. These α-Fe_2O_3 nuclei are quite unstable because of their high surface energy and tend to aggregate rapidly to form primary nanocrystals.[25] The formed primary crystals recrystallize to produce the final crystals. It has been widely accepted that functional molecules adsorbed on the surface of nanoparticles have an important influence on their self-assembly behavior.[26,27] The preferential absorption of molecules and ions in solution to different crystal faces directs the growth of particles into various shapes by controlling the growth rates along different crystal axes.[19,28,29] The amino acids normally adsorb on the α-Fe_2O_3 surface via bridged chelate surface-complex formation through the –COOH and –NH_2 groups.[30] As shown in Fig. 10, the four kinds of amino acids differ from each other in the side chain attached to their alpha carbon. For glutamic acid, aspartic acid and asparagine, they have something in common: all of them contain carbon–oxygen double bond (C=O) in the side chain. Spindle-like α-Fe_2O_3 nanoparticles can be prepared in the presence of these three kinds of amino acids. However, lysine just contains an amino group in the long side chain without carbon–oxygen double bond.

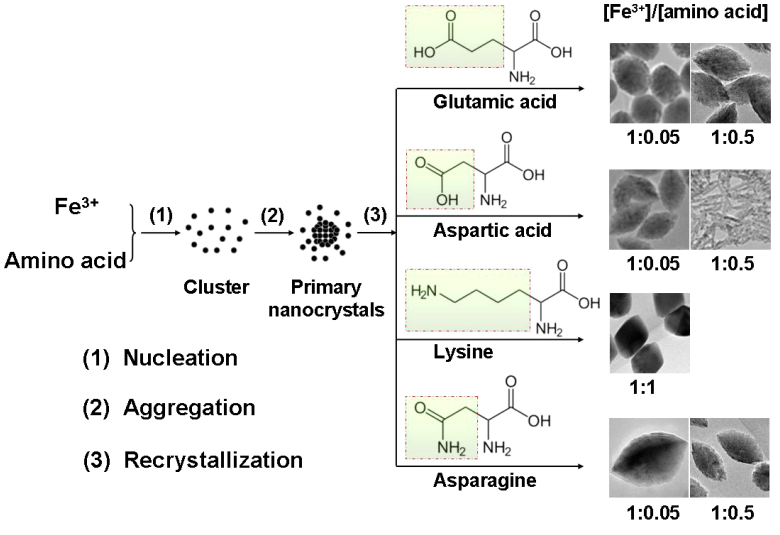

Fig. 10. Schematic illustration for α-Fe_2O_3 nanoparticles growth in the presence of amino acids. The results using asparagine to prepare α-Fe_2O_3 were cited from our previous work.[13]

The obtained α-Fe_2O_3 nanoparticles in the presence of lysine are rhombohedral. We can deduce that the carbon–oxygen double bond in the side chain has important role in synthesis of spindle-like α-Fe_2O_3 nanoparticles. Compared with the results of α-Fe_2O_3 prepared with glutamic acid, aspartic acid and asparagine in the same $[Fe^{3+}]$/[amino acid] molar ratio (1:0.5), it seems that aspartic acid (rod) is more effective in controlling the morphology of α-Fe_2O_3 nanoparticles than glutamic acid (spindle) and asparagine (spindle), which may be caused by the stronger interaction between aspartic acid and α-Fe_2O_3 crystals. According to the molecular formulas shown in Fig. 10, glutamic acid just contains one more methylene group (–CH_2–) in the side chain than aspartic acid, while asparagine contains another amino group in the side chain. It appears that long side chain or amino group in the side chain can reduce the interaction between amino acid and Fe_2O_3 crystals. In general, the different numbers of amine and carboxyl groups have great impact on the shapes of α-Fe_2O_3 crystal by affecting the degrees of chelating, hydrolysis and adsorption/desorption of the specific molecules on certain surfaces of a crystal.

As known, the final nanocrystal size is highly dependent on the supersaturation of the primary seeds. At high concentration of amino acids and lower aging temperature, the resultant crystals have smaller particle sizes, which is due to both the adsorbed amino acid molecules on certain facets that slow down the crystal growth and the steric effect of larger number of amino acid molecules limiting the growth of the crystals. At last, the resultant crystals have smaller particle sizes. However, if the amount of amino acids is too high, defective α-Fe_2O_3 nanoparticles are produced (see Figs. 6(b) and 6(c)), which is in agreement with a publication that the potency and morphological specificity of the additives are lost at high concentration where nonspecific binding becomes paramount.[31] In addition, at higher aging temperature the nucleation and high growth rates to some extent mask the influence of the additive. Thus, the sizes and shapes of the products are not so well-controlled any more than at lower synthesis temperature.

4. Conclusion

Uniform α-Fe_2O_3 nanoparticles with well-defined shape and size have been synthesized with various amino acids as additives. The influence of the type and amount of amino acids and the reaction temperature were investigated. It turned out that the type and amount of amino acids play a crucial role in governing the growth of certain shapes and sizes of the α-Fe_2O_3 products. By changing the reaction conditions, uniform and monodispersed α-Fe_2O_3 nanoparticles with different shapes can be obtained.

Acknowledgments

The project was supported by the Key Project of Chinese Ministry of Education (No. 108138) and the State Key Laboratory of Fine Chemicals, Dalian University of Technology (DUT). The authors would like to thank the basic funding provided by Max-Planck-Institut für Kohlenforschung (MPIKOFO), the DFG SFB 558 and DUT funding for the DUT-MPIKOFO joint research center.

References

1. P. Landon, J. Ferguson and B. E. Solsona, *J. Mater. Chem.* **16**, 199 (2006).
2. J. Chen, L. Xu, W. Li and X. Gou, *Adv. Mater.* **17**, 582 (2005).
3. I. Cesar, A. Kay, J. G. Martinez and M. Grätzel, *J. Am. Chem. Soc.* **128**, 4582 (2006).
4. X. Liang, X. Wang, J. Zhuang, Y. Chen, D. Wang and Y. Li, *Adv. Funct. Mater.* **16**, 1805 (2006).
5. G. J. Muench, S. Arajs and E. Matijevic, *Phys. Stat. Sol. A* **92**, 187 (1985).
6. K. Woo, H. J. Lee, J. P. Ahn and Y. S. Park, *Adv. Mater.* **15**, 1761 (2003).
7. S. B. Wang, Y. L. Min and S. H. Yu, *J. Phys. Chem. C* **111**, 3551 (2007).
8. C. J. Jia, L. D. Sun, Z. G. Yan, L. P. You, F. Luo, X. D. Han, Y. C. Pang, Z. Zhang and C. H. Yan, *Angew. Chem. Int. Ed.* **44**, 4328 (2005).
9. X. Wen, S. Wang, Y. Ding, Z. L. Wang and S. Yang, *J. Phys. Chem. B* **109**, 215 (2005).
10. X. Hu, J. C. Yu, J. Gong, Q. Li and G. Li, *Adv. Mater.* **19**, 2324 (2007).
11. R. D. Zysler, *Phys. Rev. B* **68**, 212408 (2003).
12. L. Liu, H. Z. Kou, W. Mo, H. Liu and Y. Wang, *J. Phys. Chem. B* **110**, 15218 (2006).
13. G.-H. Wang, W.-C. Li, K.-M. Jia, B. Spliethoff, F. Schüth and A.-H. Lu, *Appl. Catal. A* **364**, 42 (2009).
14. Z. Zhong, J. Teo, M. Lin and J. Ho, *Top. Catal.* **49**, 216 (2008).
15. X. Liu, G. Qiu, A. Yan, Z. Wang and X. Li, *J. Alloys Compounds* **433**, 216 (2007).
16. Y. S. Han, S. M. Yoon and D. K. Kim, *Bull. Kor. Chem. Soc.* **21**, 1193 (2000).

17. X. Wang, J. Zhuang, Q. Peng and Y. D. Li, *Nature* **437**, 121 (2005).
18. M. Siskin and A. R. Katritzky, *Science* **254**, 231 (1991).
19. Z. Pu, M. Cao, J. Yang, K. Huang and C. Hu, *Nanotechnology* **17**, 799 (2006).
20. B. Jia and L. Gao, *Cryst. Growth Des.* **8**, 1372 (2008).
21. H. Cao, G. Wang, V. Zhang, L. Liang, S. Zhang and X. Zhang, *Chem. Phys. Chem.* **7**, 1897 (2006).
22. K. Kandori, M. Sakai, S. Inoue and T. Ishikawa, *J. Coll. Interf. Sci.* **293**, 108 (2006).
23. S. Music, S. Krehula, S. Popovic and Z. Skoko, *Mater. Lett.* **57**, 1096 (2003).
24. T. P. Raming, A. J. A. Winnubst, C. M. van Kats and A. P. Philipse, *J. Coll. Interf. Sci.* **249**, 346 (2002).
25. X. Hu and J. C. Yu, *Adv. Funct. Mater.* **18**, 880 (2008).
26. H. Cao, X. Qian, C. Wang, X. Ma, J. Yin and Z. Zhu, *J. Am. Chem. Soc.* **127**, 16024 (2005).
27. J. Yue, X. Jiang, Q. Zeng and A. Yu, *Solid State Sci.* **12**, 1152 (2010).
28. J. Aizenberg, A. J. Black and G. M. Whitesides, *Nature* **398**, 495 (1999).
29. V. F. Puntes, K. M. Krishnan and A. P. Alivisatos, *Science* **291**, 2115 (2001).
30. J. Bandara, K. Tennakone and J. Kiwi, *Langmuir* **17**, 3964 (2001).
31. S. Mann, *Angew. Chem. Int. Ed.* **39**, 3392 (2000).